ACS APPLIED MATERIALS & INTERFACES

Research Article

www.acsami.org

Double Metal Ions Synergistic Effect in Hierarchical Multiple Sulfide Microflowers for Enhanced Supercapacitor Performance

Yang Gao,[†] Liwei Mi,*[,‡,§] Wutao Wei,[‡] Shizhong Cui,[‡] Zhi Zheng,[§] Hongwei Hou,[†] and Weihua Chen*[,†]

[†]College of Chemistry and Molecular Engineering, Zhengzhou University, Zhengzhou, Henan 450001, P. R. China

[‡]Center for Advanced Materials Research, Zhongyuan University of Technology, Zhengzhou, Henan 450007, P. R. China

[§]Key Laboratory for Micro-Nano Energy Storage and Conversion Materials of Henan Province, Institute of Surface Micro and Nano Materials, Xuchang University, Xuchang, Henan 461000, P. R. China

Supporting Information

ABSTRACT: In this paper, the design, synthesis, and measurement of a new and hierarchically structured series of $Ni_xCo_{1-x}S_{1.097}$ electroactive materials are reported. The materials were synthesized through an ion-exchange process using hierarchically structured $CoS_{1.097}$ as precursors, and a strategy utilizing the synergistic effect of double metal ions was developed. Two complementary metal ions were used to enhance the performance of electrode materials. The specific capacitance of the electroactive materials was continuously improved by increasing the nickel ion content, and the electric conductivity was also enhanced when the cobalt ion was varied. Experimental results showed that the nickel ion content in $Ni_xCo_{1-x}S_{1.097}$ could be adjusted from $x = 0$ to 0.48. Specifically, when $x = 0.48$, the composite exhibited a remarkable maximum specific capacitance approximately 5 times higher than that of the $CoS_{1.097}$ precursors at a current density of 0.5 A g^{-1}. Furthermore, the specific capacitance of $Ni_{0.48}Co_{0.52}S_{1.097}$ electrodes that were modified with reduced graphene oxide could reach to 1152 and 971 F g^{-1} at current densities of 0.5 and 20 A g^{-1} and showed remarkably higher electrochemical performance than the unmodified electrodes because of their enhanced electrical conductivity. Thus, the strategy utilizing the synergistic effect of double metal ions is an alternative technique to fabricate high-performance electrode materials for supercapacitors and lithium ion batteries.

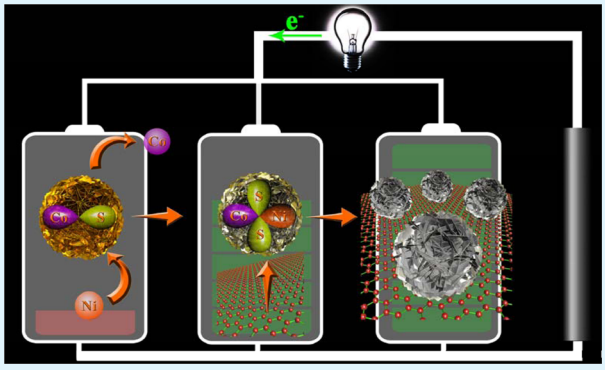

KEYWORDS: *metal sulfides, synergistic effect, supercapacitors, high rate performance*

INTRODUCTION

High-performance structured materials have drawn particular attention because of their potential applications in renewable energy technology,[1,2] addressing the issues of effective energy storage and conversion.[3−5] New techniques for material fabrication are one of the core issues for advancement of science and technology.[6−8] Currently, the most widely used approaches have enabled syntheses of materials with unique morphology and desirable composition.[9,10] However, the time-consuming and labor-intensive fabrication process limit the large-scale practical application of these approaches. Therefore, exploring a simple and effective strategy to fabricate high-performance materials is necessary to satisfy the projected energy requirements.

Transition-metal oxides, hydroxides, and their compounds have been widely explored as high-performance supercapacitor materials because of their rich valence states for a reversible Faradaic reaction.[11−19] The reported transition-metal oxides, such as RuO_2,[15] MnO_x,[17] NiO,[18] and Co_xO_y,[16,19] have been intensively and successfully examined as advanced electrode materials for supercapacitors. However, the relatively high cost and low abundance of RuO_2 materials have considerably limited their widespread use in supercapacitors. In addition, transition-metal oxides, such as MnO_x, NiO, and Co_xO_y, exhibit poor electron conductivity that cannot support fast electron transport, which is necessary for high-performance materials.[12,17−19] To overcome this limitation, cobalt sulfides and nickel sulfides have been extensively investigated as new electrode materials for supercapacitors because of their abundance, low cost, and environmental friendliness.[20−23,42−44]

Zheng and co-workers[24] reported that flowerlike NiS electrodes display a specific capacitance as high as 965.98 F g^{-1} at a current density of 0.5 A g^{-1}. Lou and co-workers[25] fabricated CoS_2 ellipsoids as positive materials that exhibit a supercapacitive performance of 1040 F g^{-1} at 0.5 A g^{-1} and 750 F g^{-1} at 5 A g^{-1}. In addition, the current authors previously focused on nestlike Ni_3S_2@NiS for supercapacitors with a specific capacitance of 516 F g^{-1} at a current density of 0.5 A

Received: December 11, 2014
Accepted: January 27, 2015
Published: January 27, 2015

DOI: 10.1021/am508747m
ACS Appl. Mater. Interfaces 2015, 7, 4311−4319

g^{-1}.[9] Individual nickel- and cobalt-based electrodes possess high theoretical capacity, but the poor intrinsic conductivity still limits their rate capability.[9,24,25] Nevertheless, ternary sulfides, such as nickel−cobalt sulfides, exhibit an electric conductivity that is approximately 2 orders of magnitude higher than corresponding oxides[20,23] and much higher than those of single-component sulfides.[26] Therefore, the integration of Ni and Co electrode materials results in higher capacitance and rate capability than an individual metal compound.

The present synthesis method of large-scale, high-performance electroactive materials for supercapacitors is based on the synergistic effect of double metal ions. This strategy carefully combines two kinds of complementary advantageous metal ions and provides a highly efficient route to synthesize a wide variety of materials with enhanced performance. Through this strategy, 3D hierarchically structured $Ni_xCo_{1-x}S_{1.987}$ (x = 0−0.48) microspheres have been successfully synthesized, and a notable enhancement on both capacitance and rate capability over $CoS_{1.097}$ precursors has been exhibited. The superior electrochemical performance can be ascribed to three main factors. First, the synergistic effect of cobalt and nickel ions in ternary sulfides provides richer redox chemistry than those of the corresponding individual binary sulfides, which possess higher theoretical capacity.[27] Second, the hierarchical structure provides a high specific surface area and endows it with more active sites, which ensures efficient redox reactions and fast ion transport.[28] Third, a small nickel ion that could enable the activity of cobalt ion significantly increases in ternary sulfides, which remarkably enhances electrochemical performance. Furthermore, the electrochemical performance of $Ni_xCo_{1-x}S_{1.097}$ (x = 0−0.48) could be continuously and meticulously modulated by adjusting the molar ratios of nickel and cobalt ions. $Ni_{0.48}Co_{0.52}S_{1.097}$ microspheres can remarkably deliver a high specific capacitance of 867.0 F g^{-1} at a current density of 0.5 A g^{-1} and a good rate capability with 69% capacitance retention at a high current density of 20 A g^{-1}. For comparison, electrodes with pure $CoS_{1.097}$ were also examined. The supercapacitors based on the $CoS_{1.097}$ microspheres present a low specific capacitance of 186.0 F g^{-1} at a current density of 0.5 A g^{-1}. The results demonstrate that the synergistic effect of double metal ions could effectively enhance the electrochemical performance of electrode materials.

The conductivity of active materials plays an extremely important role in enhancing the electrochemical performance of materials. Sheetlike graphene has been intensively investigated as a backbone to support electrode materials for high-performance supercapacitors because of its large surface area, high mechanical strength, and good electric conductivity.[29,30] To improve the electrochemical performance of the electrode materials, advanced active materials of $Ni_xCo_{1-x}S_{1.097}$ (x = 0−0.48) directly grown on reduced graphene oxide (rGO) graphene sheets were synthesized to utilize the conductive substrate and the synergistic effect of double metal ions. The as-synthesized $Ni_xCo_{1-x}S_{1.097}$−rGO exhibits enhanced specific capacitance and rate capability compared with the $Ni_xCo_{1-x}S_{1.097}$ electrodes. More significantly, this strategy is suitable for scalable and controllable production. The novel strategy presented in this paper could also be applied to fabricate other double-metal electrodes.

EXPERIMENTAL SECTION

Materials. All the chemicals and solvents used were of analytic grade purity and used without further purification.

Synthesis of 3D Hierarchically Structured $CoS_{1.097}$ Microspheres. The 3D hierarchically structured $CoS_{1.097}$ microspheres have been successfully fabricated by a solvothermal reaction using simple cobalt coordination compounds as precursors. Typically, single crystals of $\{[NaCo_3(TMA)_2(\mu_3\text{-}OH)(\mu_2\text{-}H_2O)_4(H_2O)_7]\cdot 1.5H_2O\}_n$ were obtained via the reaction of cobalt(II) sulfate with trimesic acid (H_3TMA = 1,3,5-benzenetricarboxylic acid) under pH 6.9, where the pH was adjusted using 0.5 M NaOH.[41] Cobalt coordination compounds (1 mmol) were placed in 5 mL of ethylene glycol solvent in a glass bottle, and then 0.25 mL of glacial acetic acid was added into the bottle with heating and stirring. Concomitantly, 2 mmol of thiourea was dissolved in 11 mL of ethanediamine and then added dropwise to the mixture in the glass bottle. After being stirred for 8 h, the mixture was transferred to a 20 mL Teflon-sealed autoclave, maintained at 160 °C for 24 h, and cooled to room temperature naturally. The product was removed from the solution and repeatedly washed several times with deionized water and 95% ethanol. Finally, the as-synthesized materials were dried in a vacuum oven at 60 °C for 8 h.

We investigated the effects of the pH of the solvent system to study the growth mechanism of the 3D hierarchically structured $CoS_{1.097}$ crystals using our synthesis method. Several parallel experiments were performed with the same synthesis conditions but with the amounts of acetic acid varied. The amounts of acetic acid added for materials **2**, **3**, **4**, and **5** were 0, 0.25, 0.75, and 1.25 mL, respectively.

Synthesis of 3D Hierarchically Structured $Ni_xCo_{1-x}S_{1.097}$ Microspheres. The 3D hierarchically structured $Ni_xCo_{1-x}S_{1.097}$ microspheres were prepared by the nickel ion exchange method using as-synthesized $CoS_{1.097}$ materials as the precursor. In order to obtain optimized product performance, a time-dependent experiment was performed. In this process, 1 mmol of $CoS_{1.097}$ was immersed in an aqueous solution of nickel nitrate for different replacement durations (10, 20, 30, 40, 50, 60, 70, and 180 min) at 160 °C under hydrothermal conditions. The resulting products, $Ni_{0.10}Co_{0.90}S_{1.097}$, $Ni_{0.15}Co_{0.85}S_{1.097}$, $Ni_{22}Co_{0.78}S_{1.097}$, $Ni_{0.28}Co_{0.72}S_{1.097}$, $Ni_{0.34}Co_{0.66}S_{1.097}$, $Ni_{0.43}Co_{0.57}S_{1.097}$, $Ni_{0.45}Co_{0.55}S_{1.097}$, and $Ni_xCo_{1-x}S_{1.097}$−$Ni(OH)_2$ were prepared by adjusting the concentration of nickel nitrate (Ni/Co ratio = 2/1).

We also investigate the effect of the concentration of nickel nitrate on the products. Materials $Ni_{0.25}Co_{0.75}S_{1.097}$, $Ni_{0.46}Co_{0.54}S_{1.097}$, $Ni_{0.48}Co_{0.52}S_{1.097}$, and $Ni_xCo_{1-x}S_{1.097}$−$Ni(OH)_2$ were prepared by a method similar to that of the material $Ni_{0.43}Co_{0.57}S_{1.097}$, but the concentration of nickel nitrate was adjusted to get the Ni/Co atomic ratio to 1:1, 3:1, 4:1, and 5:1. Finally, the as-prepared materials were centrifuged, washed several times with deionized water and 95% ethanol, dried in a vacuum oven at 60 °C for 8 h, and collected for further characterization.

Synthesis of $Ni_xCo_{1-x}S_{1.097}$−Reduced Graphite Oxide (rGO) Hybrid Materials. The $Ni_xCo_{1-x}S_{1.097}$−rGO hybrid materials were prepared by a hydrothermal method. A certain amount of $Ni_xCo_{1-x}S_{1.097}$ (x = 0−0.48) materials and 8 mL of aqueous solutions of rGO sheets were added to a 20 mL Teflon-sealed autoclave and maintained at 160 °C for 3 h. The amounts of rGO in the final composites were controlled to be ∼5 wt %.

Characterization. X-ray diffraction (XRD) patterns were obtained with a Bruker D8 Advance X-ray powder diffractometer using Cu Kα irradiation at a scan rate of 0.1° s^{-1}. XRD measurements of $CoS_{1.097}$ and $Ni_xCo_yS_{1.097}$ materials were performed within $10° \le 2\theta \le 80°$. The morphologies and sizes of the as-prepared $CoS_{1.097}$ and $Ni_xCo_yS_{1.097}$ microspheres were characterized with a Zeiss EVO LS-15 scanning electron microscope (SEM) equipped with an energy-dispersive X-ray spectroscopy (EDS) system. The nanostructures of the resulting materials were recorded with a JEOL JEM-2010 transmission electron microscope (TEM). The X-ray photoelectron spectroscopy (XPS) of the as-obtained $Ni_xCo_yS_{1.097}$ microflower was done using a Kratos AXIS ULTRA X-ray photoelectron microscope with Al Kα X-rays as the excitation source. N_2 adsorption isotherms were measured at 77 K on a Micromeritics ASAP2420 instrument. The specific surface areas were determined using the Brunauer−Emmett−Teller (BET) method.

DOI: 10.1021/am508747m
ACS Appl. Mater. Interfaces 2015, 7, 4311−4319

Electrochemical Performance Test. Cyclic voltammetry (CV) measurements were carried out a CHI604E electrochemical workstation (Chenhua, Shanghai, China) at voltage scanning rates ranging from 1 to 300 mV s^{-1}. Electrochemical measurements were conducted in a three-electrode mode in 2 M KOH electrolyte. In this case, 80% of the active material and 10% each of carbon black and polyvinylidene difluoride (PVDF) were uniformly mixed and then cast onto a nickel foam, which was used as a working electrode. A saturated Hg/HgO electrode and a platinum plate were employed as the reference and counter electrode, respectively. The galvanostatic charge−discharge tests were conducted with current densities of 0.5, 1, 2, 5, 10, and 20 A g^{-1} using a LAND battery test system (CT2001A model).

RESULTS AND DISCUSSION

Advanced active materials with regular structure are highly desirable for energy storage systems because their electrochemical performance is superior to those with irregular architecture.[31,32] Hierarchically structured electrodes have recently received great attention for supercapacitors because of their increased active surface area as well as short electron and ion transport pathways.[28] Crystal phases and novel architecture can be synthesized using an exciting crystal lattice as a template.[33] Electrochemical properties of materials depend not only on the composition of the electrode materials but also on the architecture of these electrodes. Thus, controllable syntheses of electrodes with desirable composition and hierarchical architecture are expected to have remarkable potential for generating high-performance supercapacitors. In this study, large-scale, 3D hierarchically structured $CoS_{1.097}$ microspheres were first fabricated using cobalt coordination compounds as precursors via a simple solvothermal reaction at 160 °C for 24 h. Comparing with simple metal salts, there are several advantages to synthesize $CoS_{1.097}$ by using the coordination compound as a precursor. First, the formation of coordination bonds could delay the release rate of the central metal ion as well as increase the capability for an ordered arrangement of the metal ions,[45] which helps in controlling the morphology of the products. Second, the auxiliary ligands in the complex serve as a reaction-active agent or auxiliary agent after dissociation from the complex. The morphology of the as-prepared $CoS_{1.097}$ was characterized using scanning electron microscopy (SEM). The low-magnification SEM image of $CoS_{1.097}$ (Figure 1a) shows a uniform microsphere with a diameter of 16−18 μm. The magnified SEM images of $CoS_{1.097}$ (Figure 1b) revealed that each microsphere possessed a hierarchical architecture assembled by numerous bent nanosheets. This unique 3D hierarchical architecture could provide a sufficient electrolyte−electrode interface for fast diffusion and reaction because of its large specific surface area (Figure S1, Supporting Information) and multiple active sites.

The crystallographic structures of the as-obtained products were determined by X-ray diffraction (XRD). A typical XRD pattern for 3D hierarchically structured $CoS_{1.097}$ microsphere is shown in Figure 1c. All of the observed diffraction peaks can be perfectly indexed to the standard data of $CoS_{1.097}$ phase (JCPDS no. 19-0366) with hexagonal structure in space group *p*63/*mmc* (No. 194), indicating that the as-obtained $CoS_{1.097}$ crystals have a pure phase. The composition of the as-obtained products was determined by energy-dispersive X-ray spectroscopy (EDX); the Co/S ratio was found to be 48.63:51.37, which is very close to the stoichiometric ratio of 1:1.097 (Figure 1d). Moreover, high-resolution TEM (HRTEM) images were used to illustrate the geometrical structure of the nanosheets on the $CoS_{1.097}$ surface (Figure 1e). The distance of

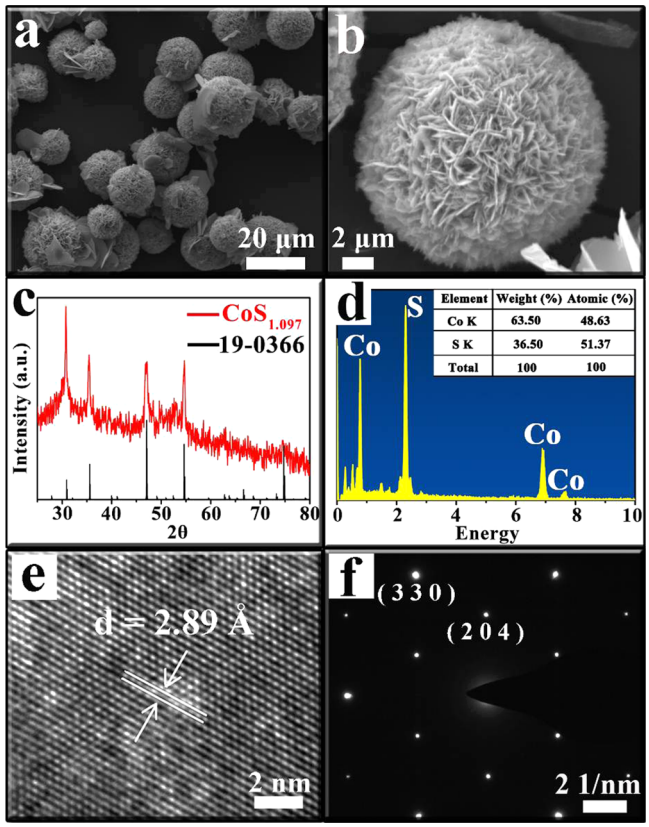

Figure 1. Characterization of the $CoS_{1.097}$ microspheres by SEM (a, b), XRD (c), EDX (d), and TEM (e, f).

the adjacent lattice fringes is 2.89 Å, which is consistent with the (204) plane of $CoS_{1.097}$ crystals (JCPDS no. 19-0366). The ordered lattice fringes suggest a highly crystalline nature for the $CoS_{1.097}$ product. The selected area electron diffraction (SAED) pattern (Figure 1f) confirms the single crystallinity of the $CoS_{1.097}$ nanoplates. The 0.289 and 0.168 nm lattice spacings correspond to the (204) and (330) planes of the $CoS_{1.097}$ phase.

Acidic conditions are preferred in generating the 3D hierarchically structured $CoS_{1.097}$ microspheres. To examine the influence of acetic acid content on the final products, several parallel experiments were performed systematically with various volumes of concentrated acetic acid. SEM images and XRD patterns of the products obtained with different amounts of acetic acid at 160 °C for 24 h are shown in Figure S2 (Supporting Information). With the absence of acetic acid, as-obtained material **2** displayed an irregular architecture of assembled hexagonal plates. With 0.25 mL acetic acid, material **3** changed into a 3D hierarchical microsphere. These results may be attributed to the presence of acetic acid, which provided an effective binder for the formation of 2D petals and then the 3D hierarchical microflower. With an increased amount of acetic acid, the 2D petal-like building units of the microsphere continually increased, which then evolved into a peonylike microflower. Thus, 0.25 mL acetic acid was added to the mixture solution to obtain 3D hierarchical microspheres.

The rational design of electrodes with hierarchical architecture is an effective technique to enhance electrochemical performance. In this study, a 3D hierarchically structured $CoS_{1.097}$ microsphere has been successfully synthesized and used as electrodes for supercapacitors. Experimental

DOI: 10.1021/am508747m
ACS Appl. Mater. Interfaces 2015, 7, 4311−4319

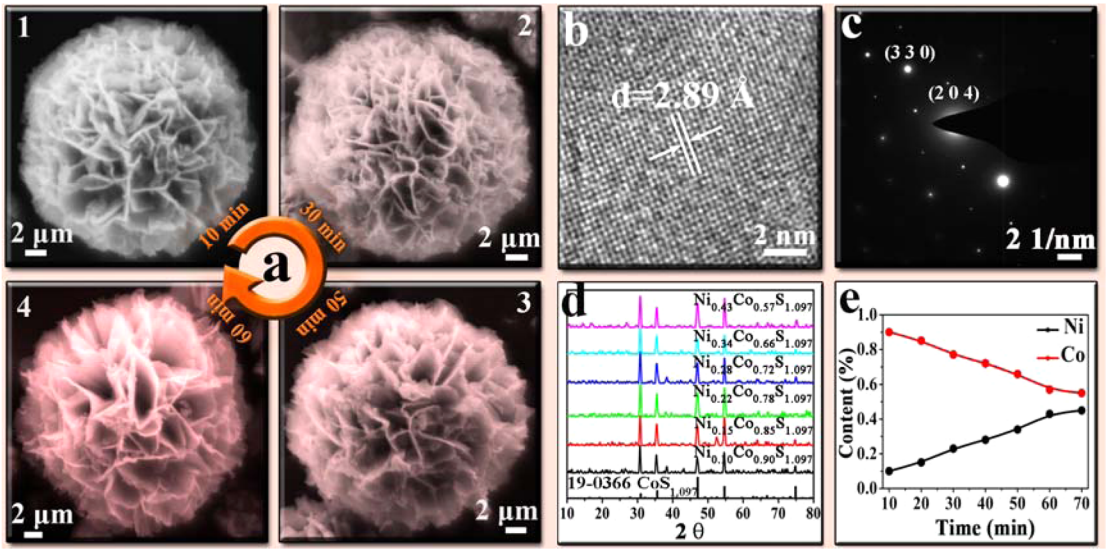

Figure 2. SEM images of (a1) $Ni_{0.10}Co_{0.90}S_{1.097}$, (a2) $Ni_{22}Co_{0.78}S_{1.097}$, (a3) $Ni_{0.34}Co_{0.66}S_{1.097}$, and (a4) $Ni_{0.43}Co_{0.57}S_{1.097}$. (b) HRTEM images of $Ni_{0.43}Co_{0.57}S_{1.097}$. (c) SAED pattern of $Ni_{0.43}Co_{0.57}S_{1.097}$. (d) XRD patterns of $Ni_xCo_{1-x}S_{1.097}$ (x = 0.10−0.43). (e) Curves of the element ratio of Co and Ni in $Ni_xCo_{1-x}S_{1.097}$ (x = 0.10−0.45), which was obtained by EDX measure.

results showed that the as-synthesized $CoS_{1.097}$ electrode materials exhibited low specific capacitance and low rate capability, which limit the application of these materials. However, ternary metal sulfides possess better electrical conductivity and higher theoretical capacitance than single metal sulfides, because of the synergistic effect of the double metal ions in sulfide structures. To obtain high-performance supercapacitor electrodes, a novel strategy to fabricate electrodes for supercapacitors by the synergistic effect of double metal ions is reported. Ni ion, as a helpful cation for supercapacitors, was introduced into $CoS_{1.097}$ materials to prepare $Ni_xCo_{1-x}S_{1.097}$ (x = 0.10−0.48) electrode materials. In this process, $Ni_xCo_{1-x}S_{1.097}$ electrodes with adjustable composition could be obtained through the cation-exchange reaction between $CoS_{1.097}$ microsphere and nickel nitrate. A molar ratio of 2:1 of nickel−cobalt ions in solution in solid $CoS_{1.097}$ was used for different replacement durations (10, 20, 30, 40, 50, 60, 70, and 180 min) at 160 °C. The general advantage of this synthetic procedure is the use of nickel nitrate as an inexpensive starting material and water as an environmentally friendly solvent compared with the traditional synthetic pathway, in which expensive compounds such as organic solvent or organometallics are used. The SEM images of $Ni_{0.10}Co_{0.90}S_{1.097}$, $Ni_{22}Co_{0.78}S_{1.097}$, $Ni_{0.34}Co_{0.66}S_{1.097}$, and $Ni_{0.43}Co_{0.57}S_{1.097}$, which were prepared at 160 °C for 10, 30, 50, and 60 min, were used as representatives (Figure 2a1−a4). $Ni_xCo_{1-x}S_{1.097}$ electrodes expectedly inherited the morphology of $CoS_{1.097}$ to the maximum degree, with only a less-compact nanosheet as the difference. The HRTEM image (Figure 2b) shows that $Ni_{0.43}Co_{0.57}S_{1.097}$ materials are highly crystalline. The lattice fringe spacing was measured to be 2.89 Å, which corresponded to the $CoS_{1.097}$ plane (JCPDS no. 19-0366). According to the SAED pattern (Figure 2c), the $Ni_{0.43}Co_{0.57}S_{1.097}$ could also be identified as $CoS_{1.097}$ (JCPDS No. 19-0366). The XRD patterns of the $Ni_xCo_{1-x}S_{1.097}$ (x = 0.10−0.43) (Figure 2d) were similar to the standard patterns of $CoS_{1.097}$, indicating that the mixed nickel−cobalt sulfide adopts the hexagonal structure with similar lattice constants. This condition suggests the occurrence of in situ solid-state displacement reactions. According to the EDX results, the molar ratios of nickel to cobalt in materials $Ni_xCo_{1-x}S_{1.097}$ were 0.10:0.90, 0.15:0.85, 0.22:0.78, 0.28:0.72, 0.34:0.66, 0.43:0.57, and 0.45:0.55 (Figure 2e). However, as the reaction time reached 180 min, several impurity peaks of $Ni(OH)_2$ were found in the XRD of $Ni_xCo_{1-x}S_{1.097}$ (Figure S3, Supporting Information). The corresponding EDX measurements further confirmed this result (Figure S4, Supporting Information). This phenomenon finally resulted in the formation of $Ni_xCo_{1-x}S_{1.097}$ microsphere with adjustable composition.

The composition of $Ni_xCo_{1-x}S_{1.097}$ was also adjusted by varying the concentration of the reactants. When the replacement duration was 60 min and the molar ratios of Ni/Co were changed up and down to 4:1, 3:1, and 1:1, then $Ni_{0.48}Co_{0.52}S_{1.097}$, $Ni_{0.46}Co_{0.54}S_{1.097}$, and $Ni_{0.25}Co_{0.75}S_{1.097}$ materials were obtained with different Ni:Co atomic ratios of 0.25:0.75, 0.46:0.54, and 0.48:0.52 based on the EDX results. The morphologies of the as-prepared $Ni_{0.25}Co_{0.75}S_{1.097}$, $Ni_{0.46}Co_{0.54}S_{1.097}$, and $Ni_{0.48}Co_{0.52}S_{1.097}$ were characterized via SEM (Figure S5a−c, Supporting Information). The morphologies of $Ni_{0.25}Co_{0.75}S_{1.097}$, $Ni_{0.46}Co_{0.54}S_{1.097}$, and $Ni_{0.48}Co_{0.52}S_{1.097}$ basically remained unchanged and corresponded to that of $CoS_{1.097}$. The crystal nature was further confirmed by XRD data (Figure S5d, Supporting Information). However, several impurity peaks appeared when the Ni/Co molar ratio was 5:1 at 60 min reaction (Figures S6 and S7, Supporting Information). When the reaction time was 60 min and Ni/Co molar ratios were 3:1 and 4:1, the coefficient of the growth rate of the ratio of Ni/Co in material $Ni_xCo_{1-x}S_{1.097}$ was insignificant. To reduce production costs and energy consumption, the Ni/Co molar ratio of 2:1 was adopted in the synthesis of $Ni_xCo_{1-x}S_{1.097}$ with adjustable composition by the cation-exchange reaction for different replacement durations; details of the process are presented in this paper.

To obtain further information on the structure and composition of $Ni_{0.10}Co_{0.90}S_{1.097}$ and $Ni_{0.43}Co_{0.57}S_{1.097}$, X-ray photoelectron spectroscopy (XPS) was employed, and the results are presented in Figure 3. With the application of the Gaussian fitting method, the Ni 2p emission spectrum (Figure 3a,d) was fitted such that the two spin−orbit doublets characteristic of Ni^{2+} and Ni^{3+} and the two shakeup satellite

DOI: 10.1021/am508747m
ACS Appl. Mater. Interfaces 2015, 7, 4311−4319

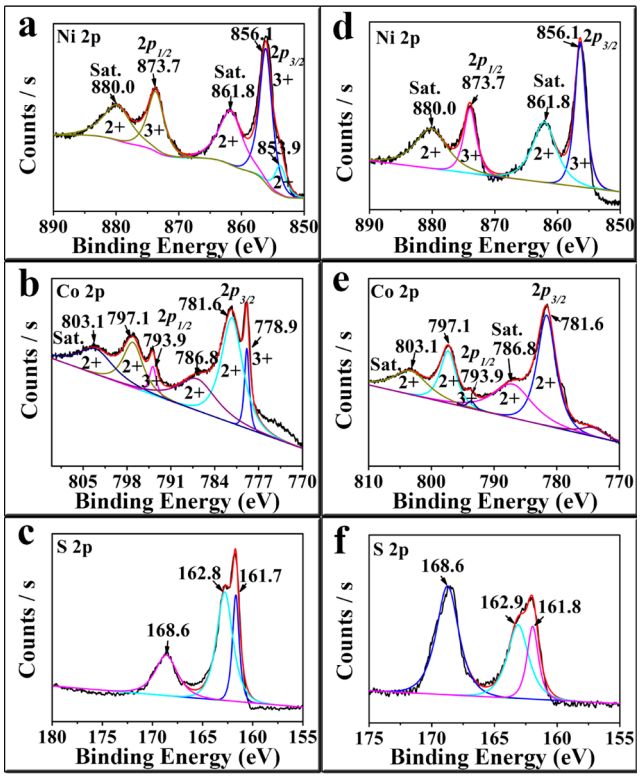

Figure 3. XPS spectra of the (a) Ni 2p (b) Co 2p, (c) S 2p for $Ni_{0.10}Co_{0.90}S_{1.097}$, (d) Ni 2p, (e) Co 2p, (f) S 2p for $Ni_{0.43}Co_{0.57}S_{1.097}$.

(identified as "Sat.") are shown. The Ni 2p spectrum can be best fitted by considering two spin−orbit doublets at 861.8 and 873.7 eV as well as at 880.0 and 856.1 eV. The doubles are assigned to Ni^{2+} and Ni^{3+},[20,26,34,35] whereas the Co $2p_{3/2}$ peaks that appeared at 781.6 and 786 eV are characteristics of Co^{2+} species, and the Co $2p_{1/3}$ peaks observed at 797.1 and 803.1 eV are characteristics of Co^{2+} and Co^{3+} species (Figure 3b,e).[34] The high-resolution spectra for the S 2p region (Figure 3c,f) show the sulfide contributions. The peak at approximately 161.8 eV is characteristic of S^{2-},[9,26] and the peak at 162.9 eV can be assigned to the sulfur ion in low coordination at the surface.[26] The S 2p peak observed at 169.0 eV could be attributed to surface sulfur with a high oxide state, such as sulfates.[20] These values approached the reported values and confirmed that Ni was introduced into $CoS_{1.097}$ and that the as-synthesized $Ni_{0.10}Co_{0.90}S_{1.097}$ and $Ni_{0.43}Co_{0.57}S_{1.097}$ had identical compositions containing Co^{2+}, Co^{3+}, Ni^{2+}, and Ni^{3+}.

To demonstrate the electrochemical superiority of nickel cobalt sulfide microspheres that were prepared through the synergistic effect of double metal ions, a comparative study with the counterpart of cobalt sulfide microspheres was performed using a standard three-electrode configuration in 2.0 M KOH. Figure S8a,b (Supporting Information) shows the typical initial cyclic voltammetry (CV) curves of the $CoS_{1.097}$ and $Ni_{0.48}Co_{0.52}S_{1.097}$ electrodes at a scan rate of 1 mV s^{-1} in a potential window of −0.1 to 0.52 V versus Hg/HgO. Obviously, the initial curve is different from the subsequent cycles. These results indicate a phase transformation from $MS_{1.097}$ to $M(OH)_2$ (M = Ni and Co species) during the first positive sweep, and only reversible redox reactions related to $M(OH)_2$/MOOH (M = Ni and Co species) and MOOH/MO_2 (M = Co species) occurred in subsequent CV tests.[9,19,36−39] The initial curves of the $Ni_{0.48}Co_{0.52}S_{1.097}$ electrode are remarkably different from that of $CoS_{1.097}$ electrodes, which could be ascribed to the synergistic contributions of cobalt and nickel double metal ions.

Figure 4a,b shows the typical CV curves of $CoS_{1.097}$ and $Ni_{0.48}Co_{0.52}S_{1.097}$ electrodes at various scan rates of 2, 5, 10, 30, 50, and 100 mV s^{-1}. With increasing scan rate, the oxidation and reduction peaks of the $Ni_xCo_{1-x}S_{1.097}$ (x = 0−0.48) electrodes gradually shifted to the right and left, respectively, which are due to fact that charge transfer kinetics is the limiting step of the reaction. A weak redox peak can be observed in the CV curves of $CoS_{1.097}$ microsphere, which suggested the poor electrochemical performance of individual cobalt sulfides. Weak anodic peaks were found at approximately 0.22−0.53 V when the scan rate was increased to 5 mV s^{-1}, and the peaks could be attributed to the oxidation of $Co(OH)_2$ to CoOOH and the conversion between CoOOH and CoO_2, whereas the cathodic peaks corresponded to the reverse process.[19,36−38] By contrast, after incorporating Ni ion into $CoS_{1.097}$ microspheres, a stronger redox peak was found in the CV curves. The CV curves of $Ni_{0.48}Co_{0.52}S_{1.097}$ showed a pair of redox peaks at 0.43 and 0.27 V at a scan rate of 5 mV s^{-1}, which corresponded to the reversible Faradaic reactions of $M(OH)_2$/MOOH (M = Ni and Co species) and MOOH/MO_2 (M = Co species).[9,19,36−39] Furthermore, the redox peak was gradually enhanced with increasing Ni content in the $Ni_xCo_{1-x}S_{1.097}$ (x = 0−0.48) microspheres, which indicates that the electrochemical performance of $Ni_{0.48}Co_{0.52}S_{1.097}$ can be enhanced and tuned by adjusting the Ni/Co molar ratios. The enhanced electrochemical performance could be attributed to the synergistic effect of double metal ions.

The galvanostatic charge−discharge measurements of the $CoS_{1.097}$ and $Ni_xCo_{1-x}S_{1.097}$ (x = 0.10−0.48) were conducted at different current densities ranging from 0.5 to 20 A g^{-1}. Figure 4c,d shows the representative plots of the charge−discharge curves in a potential window of 0−0.5 V at various current densities. Consistent with the CV results, the plateaus in the charge−discharge curves indicate the existence of the Faradaic process. The charge−discharge curves of $Ni_{0.48}Co_{0.52}S_{1.097}$ show better symmetry than those of $CoS_{1.097}$ precursors, indicating that $Ni_{0.48}Co_{0.52}S_{1.097}$ electrodes exhibit good capacitive behavior and electrochemical reversibility. The following equation is applied to calculate the specific capacitance during the galvanostatic charge−discharge process

$$C = I\Delta t/m\Delta V$$

where I is the discharge current, Δt is the time for a full discharge, m is the mass of the active material, and ΔV is the practical voltage in a full-discharge process. Figure 4e demonstrates the galvanostatic discharge process of the $CoS_{1.097}$, $Ni_{0.10}Co_{0.90}S_{1.097}$, $Ni_{0.22}Co_{0.78}S_{1.097}$, $Ni_{0.43}Co_{0.57}S_{1.097}$, $Ni_{0.46}Co_{0.54}S_{1.097}$, and $Ni_{0.48}Co_{0.52}S_{1.097}$ electrodes at a current density of 0.5 A g^{-1}. The $CoS_{1.097}$ and $Ni_xCo_{1-x}S_{1.097}$ (x = 0.10, 0.22, 0.43, 0.46, 0.48) active materials exhibited remarkable specific capacitances of 186.0, 365.7, 551.6, 690.1, 768.6, and 867 F g^{-1}, respectively, at current densities of 0.5 A g^{-1}. With the synergistic effect of cobalt and nickel in multiple sulfide nanocrystallines, the specific capacitance of electrodes can be greatly enhanced and effectively modulated through alteration of the Ni/Co molar ratios. The specific capacitance of $Ni_{0.48}Co_{0.52}S_{1.097}$ electrodes was approximately 5 times higher than that of $CoS_{1.097}$ at a current density of 0.5 A g^{-1}. The electrochemical performance of $CoS_{1.097}$, $Ni_{0.22}Co_{0.78}S_{1.097}$, and $Ni_{0.48}Co_{0.52}S_{1.097}$ under high-current conditions was also

DOI: 10.1021/am508747m
ACS Appl. Mater. Interfaces 2015, 7, 4311−4319

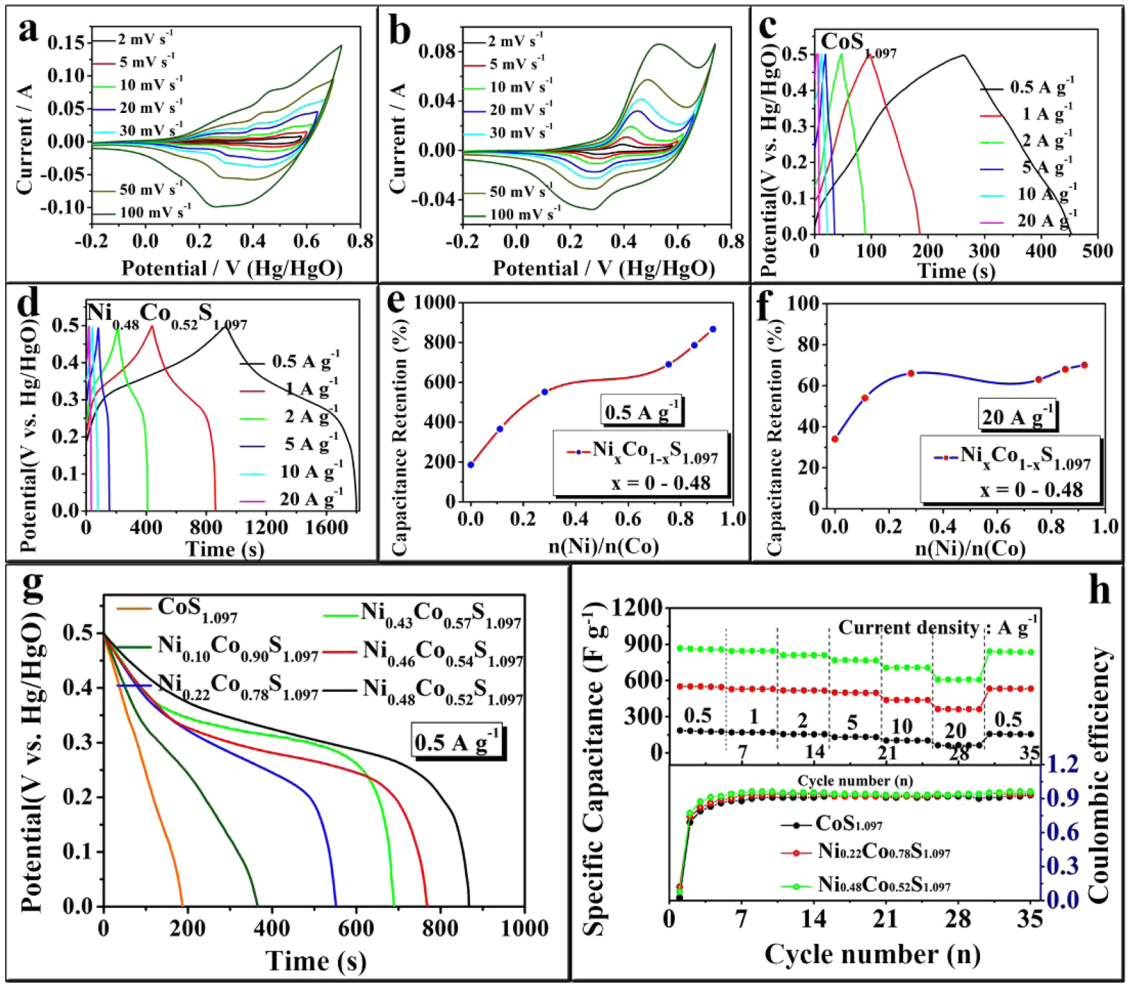

Figure 4. Electrochemical performance of the $Ni_xCo_{1-x}S_{1.097}$ (x = 0–0.48) microspheres as supercapacitor electrodes using a three-electrode configuration in 2.0 M KOH. (a, b) CV and (c, d) galvanostatic charge–discharge curves of $CoS_{1.097}$ and $Ni_{0.48}Co_{0.52}S_{1.097}$. (e) Specific capacitance at 0.5 A g^{-1} and (f) capacitance retention at 20 A g^{-1} of $Ni_xCo_{1-x}S_{1.097}$ with different Ni/Co molar ratios. (g) Galvanostatic discharge curves of $Ni_xCo_{1-x}S_{1.097}$ (x = 0, 0.10, 0.22, 0.43, 0.46, and 0.48). (h) Discharge capacitance and Coulombic efficiency curves for $CoS_{1.097}$, $Ni_{0.22}Co_{0.78}S_{1.097}$, and $Ni_{0.48}Co_{0.52}S_{1.097}$.

evaluated. Figure 4f shows the galvanostatic discharge capacitance and the Coulombic efficiency curves for the $CoS_{1.097}$, $Ni_{0.22}Co_{0.78}S_{1.097}$, and $Ni_{0.48}Co_{0.52}S_{1.097}$ electrodes at different current densities of 0.5, 1, 2, 5, 10, and 20 A g^{-1}. Noticeably, at a current density of as high as 20 A g^{-1}, $CoS_{1.097}$, $Ni_{0.22}Co_{0.78}S_{1.097}$, and $Ni_{0.48}Co_{0.52}S_{1.097}$ electrodes can still deliver corresponding specific capacitances of 63, 363, and 606 F g^{-1} (about 34%, 66%, and 69% retention, respectively). These results indicated that $Ni_xCo_{1-x}S_{1.097}$ electrodes possess relatively high specific capacitance and excellent rate performance compared with $CoS_{1.097}$ precursors. This superior electrochemical performance may be attributed to the cooperative contributions from cobalt and nickel ions and the 3D hierarchical architecture, which provided richer redox reactions, high contact surface area, and more active sites. In addition, the Coulombic efficiency of $CoS_{1.097}$, $Ni_{0.22}Co_{0.78}S_{1.097}$, and $Ni_{0.48}Co_{0.52}S_{1.097}$ is relatively high at approximately 97%, except in the first cycle because of the phase transformation reactions. Thus, 3D hierarchically structured $Ni_xCo_{1-x}S_{1.097}$ electrodes prepared by the synergistic effect of double metal ions exhibit an excellent electrochemical performance, making them potential candidates for supercapacitors.

To improve the electrochemical performance of these electrodes, 5 wt % rGO was added to modify the sulfides through a facile hydrothermal reaction. Figure 5a,b shows the TEM images of the $Ni_{0.48}Co_{0.52}S_{1.097}$ and $Ni_{0.48}Co_{0.52}S_{1.097}$–rGO electrode materials, which exhibit that the as-synthesized nickel cobalt sulfide electrode materials are microcrystalline spheres, and this microcrystalline material is enveloped in the rGO sheets, resulting in a good composite. In addition, the as-

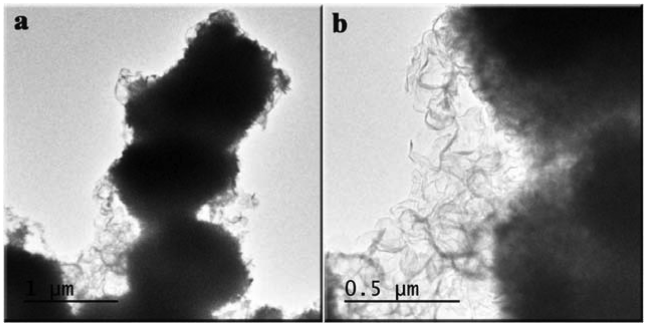

Figure 5. (a, b) TEM images of the $Ni_{0.48}Co_{0.52}S_{1.097}$ and $Ni_{0.48}Co_{0.52}S_{1.097}$–rGO electrode materials.

DOI: 10.1021/am508747m
ACS Appl. Mater. Interfaces 2015, 7, 4311–4319

obtained hierarchically structured microsphere consisted of nanocrystallines, which can be further confirmed by the TEM images in Figure S9a,b (Supporting Information). The electrochemical performance of the hybrid electrodes was evaluated by CV and galvanostatic charge−discharge techniques. Apparently, the CV curves of graphene-modified sulfides (Figures 6b and S8d, Supporting Information) exhibit a pair of

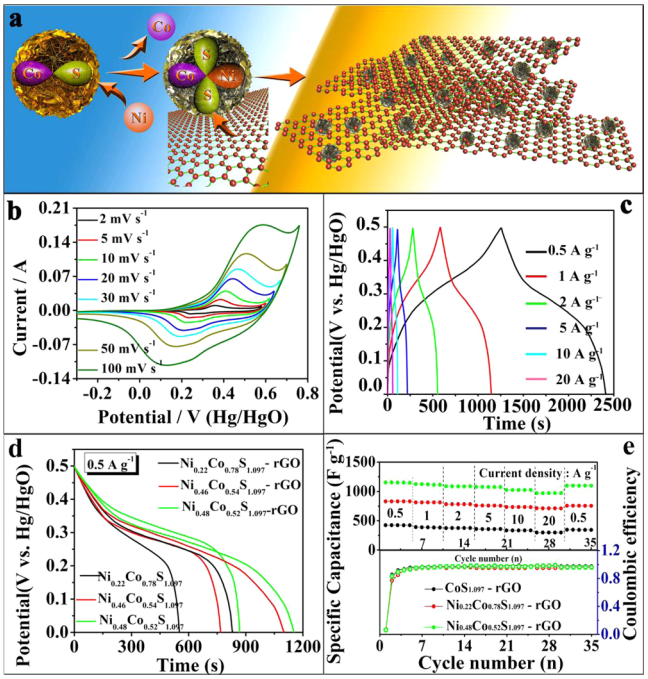

Figure 6. (a) Schematic of the fabrication of supercapacitor electrode materials from $CoS_{1.097}$ to $Ni_xCo_{1-x}S_{1.097}$ and finally to $Ni_xCo_{1-x}S_{1.097}$−rGO. (b) CV and (c) galvanostatic charge−discharge curves of $Ni_{0.48}Co_{0.52}S_{1.097}$−rGO. (d) Galvanostatic discharge curves for $Ni_xCo_{1-x}S_{1.097}$ and $Ni_xCo_{1-x}S_{1.097}$−rGO (x = 0.22, 0.46, and 0.48) at 0.5 A g^{-1}. (e) Discharge capacitance and Coulombic efficiency curves for $CoS_{1.097}$−rGO, $Ni_{0.22}Co_{0.78}S_{1.097}$−rGO, and $Ni_{0.48}Co_{0.52}S_{1.097}$−rGO.

redox peaks, which implied the presence of a reversible Faradaic reaction and pseudocapacitive behavior. Figure 6c shows the representative galvanostatic charge−discharge process of the $Ni_{0.48}Co_{0.52}S_{1.097}$−rGO at different current densities ranging from 0.5 to 20 A g^{-1}. The curves indicate that the $Ni_{0.48}Co_{0.52}S_{1.097}$−rGO electrodes possess a reversible capacitance of charge−discharge. Figure 6d shows typical discharge curves of the $Ni_xCo_{1-x}S_{1.097}$ and $Ni_xCo_{1-x}S_{1.097}$−rGO (x = 0.22, 0.46, 0.48) at a current density of 0.5 A g^{-1}. The $Ni_xCo_{1-x}S_{1.097}$−rGO electrodes possess much higher specific capacitance values than the corresponding sulfides. Furthermore, the specific capacitance and Coulombic efficiency curves for $CoS_{1.097}$−rGO, $Ni_{0.22}Co_{0.78}S_{1.097}$−rGO, and $Ni_{0.48}Co_{0.52}S_{1.097}$−rGO electrodes at increasing current densities from 0.5 to 20 A g^{-1} are shown in Figure 6e. Noticeably, the $Ni_{0.48}Co_{0.52}S_{1.097}$−rGO electrode possesses higher specific capacitance values of 1152, 1118, 1087, 1077, 1025, and 971 F g^{-1} at current densities of 0.5, 1, 2, 5, 10, and 20 A g^{-1}, respectively, than $Ni_{0.22}Co_{0.78}S_{1.097}$−rGO (from 830 to 712 F g^{-1} at from 0.5 to 20 A g^{-1}) and $CoS_{1.097}$−rGO (from 425 to 300 F g^{-1} at from 0.5 to 20 A g^{-1}). When the charge−discharge current was increased from 0.5 to 20 A g^{-1}, all of the $CoS_{1.097}$−rGO, $Ni_{0.22}Co_{0.78}S_{1.097}$−rGO, and $Ni_{0.48}Co_{0.52}S_{1.097}$−rGO electrodes exhibit excellent high-rate capability with 71%, 86%, and 84% capacitance retention, respectively. The Coulombic efficiency of the rGO-modified electrodes can reach as high as approximately 98% after the first cycle, which indicates that the $Ni_xCo_{1-x}S_{1.097}$−rGO electrodes have high charge−discharge reversibility.[40] This superior electrochemical performance could be attributed to the synergistic contributions of the cobalt and nickel ions as well as graphene.

CONCLUSION

In conclusion, a novel strategy was developed to fabricate $Ni_xCo_{1-x}S_{1.097}$ (x = 0−0.48) microspheres with a 3D hierarchical architecture using $CoS_{1.097}$ microsphere as precursors through an ion-exchange process under moderate conditions. The hierarchically structured $Ni_xCo_{1-x}S_{1.097}$ electrodes exhibited enhanced and tunable specific capacitance and rate capability. The enhanced electrochemical performance of $Ni_xCo_{1-x}S_{1.097}$ electrodes could have resulted from the hierarchical architecture and the synergistic effect of cobalt and nickel ions. Graphene was utilized to improve electrode conductivity by modifying the activity of the materials. This process resulted in an enhanced electrochemical performance. Thus, the strategy involving the synergistic effect of double metal ions in multiple sulfide nanocrystallines is an alternative technique to enhance the electrochemical performance of pseudocapacitors and batteries.

ASSOCIATED CONTENT

Supporting Information

Figures S1−S10 (BET, SEM, and TEM images, XRD and EDX patterns, and the galvanostatic charge−discharge curve of some of obtained samples). This material is available free of charge via the Internet at http://pubs.acs.org.

AUTHOR INFORMATION

Corresponding Authors

*L.M. e-mail: mlwzzu@163.com.
*W.C. e-mail: chenweih@zzu.edu.cn

Notes

The authors declare no competing financial interest.

ACKNOWLEDGMENTS

This work was supported by the National Science Foundation of China (Grant No. 21103153, 21443003 and U1407103), the Program for Innovative Research Team (in Science and Technology) in University of Henan Province (Grant No. 2012IRTSTHN021), the Specialized Research Foundation of Zhengzhou University for Young Teachers (No. 1421316035), and the Outstanding Talented Persons Foundation of Henan Province.

ABBREVIATIONS USED

CCR2 = CC chemokine receptor 2
CCL2 = CC chemokine ligand 2
CCR5 = CC chemokine receptor 5
TLC = thin layer chromatography

REFERENCES

(1) Luo, J. S.; Im, J. H.; Mayer, M. T.; Schreier, M.; Nazeeruddin, M. K.; Park, N. G.; Tilley, S. D.; Fan, H. J.; Grätzel, M. Water Photolysis at 12.3% Efficiency via Perovskite Photovoltaics and Earth-Abundant Catalysts. *Science* **2014**, *345*, 1593−1596.

DOI: 10.1021/am508747m
ACS Appl. Mater. Interfaces 2015, 7, 4311−4319

(2) Centi, G.; Quadrelli, E. A.; Perathoner, S. Catalysis for CO_2 Conversion: a Key Technology for Rapid Introduction of Renewable Energy in the Value Chain of Chemical Industries. *Energy Environ. Sci.* **2013**, *6*, 1711−1731.
(3) Chiang, Y. M. Building a Better Battery. *Science* **2010**, *330*, 1485−1486.
(4) Westover, A. S.; Tian, J. W.; Bernath, S.; Oakes, L.; Edwards, R.; Shabab, F. N.; Chatterjee, S.; Anilkumar, A. V.; Pint, C. L. A Multifunctional Load-Bearing Solid-State Supercapacitor. *Nano Lett.* **2014**, *14*, 3197−3202.
(5) Li, Y.; Fu, Z. Y.; Su, B. L. Hierarchically Structured Porous Materials for Energy Conversion and Storage. *Adv. Funct. Mater.* **2012**, *22*, 4634−4667.
(6) Austin, L. A.; Kang, B.; El-Sayed, M. A. A New Nanotechnology Technique for Determining Drug Efficacy Using Targeted Plasmonically Enhanced Single Cell Imaging Spectroscopy. *J. Am. Chem. Soc.* **2013**, *135*, 4688−4691.
(7) Wright, P. M.; Seiple, I. B.; Myers, A. G. Zur Rolle der Chemischen Synthese in der Entwicklung Antibakterieller Wirkstoffe. *Angew. Chem., Int. Ed.* **2014**, *126*, 8984−9014.
(8) Castleberry, S. A.; Li, W.; Deng, D.; Mayner, S.; Hammond, P. T. Capillary Flow Layer-by-Layer: A Microfluidic Platform for the High-Throughput Assembly and Screening of Nanolayered Film Libraries. *ACS Nano* **2014**, *8*, 6580−6589.
(9) Wei, W. T.; Mi, L. W.; Gao, Y.; Zheng, Z.; Chen, W. H.; Guan, X. X. Partial Ion-Exchange of Nickel-Sulfide-Derived Electrodes for High Performance Supercapacitors. *Chem. Mater.* **2014**, *26*, 3418−3426.
(10) Mi, L. W.; Wei, W. T.; Zheng, Z.; Gao, Y.; Liu, Y.; Chen, W. H.; Guan, X. X. Tunable Properties Induced by Ion Exchange in Multilayer Intertwined CuS Microflowers with Hierarchal Structures. *Nanoscale* **2013**, *5*, 6589−6598.
(11) Yuan, C.; Li, J.; Hou, L.; Zhang, X.; Shen, L.; Lou, X. W. Ultrathin Mesoporous $NiCo_2O_4$ Nanosheets Supported on Ni Foam as Advanced Electrodes for Supercapacitors. *Adv. Funct. Mater.* **2012**, *22*, 4592−4597.
(12) Su, Z. J.; Yang, C.; Xie, B. H.; Lin, Z. Y.; Zhang, Z. X.; Liu, J. P.; Li, B. H.; Kang, F. Y.; Wong, C. P. Scalable Fabrication of MnO_2 Nanostructure Deposited on Free-Standing Ni Nanocone Arrays for Ultrathin, Flexible, High-Performance Microsupercapacitor. *Energy Environ. Sci.* **2014**, *7*, 2652−2659.
(13) Ellis, B. L.; Knauth, P.; Djenizian, T. Three-Dimensional Self-Supported Metal Oxides for Advanced Energy Storage. *Adv. Mater.* **2014**, *26*, 3368−3397.
(14) Yang, Y.; Li, L.; Ruan, G. D.; Fei, H. L.; Xiang, C. S.; Fan, X. J.; Tour, J. M. Hydrothermally Formed Three-Dimensional Nanoporous $Ni(OH)_2$ Thin-Film Supercapacitors. *ACS Nano* **2014**, *8*, 9622−9628.
(15) Hu, C. C.; Chang, K. H.; Lin, M. C.; Wu, Y. T. Design and Tailoring of the Nanotubular Arrayed Architecture of Hydrous RuO_2 for Next Generation Supercapacitors. *Nano Lett.* **2006**, *6*, 2690−2695.
(16) Du, W.; Liu, R.; Jiang, Y.; Lu, Q.; Fan, Y.; Gao, F. Facil Synthesis of Hollow Co_3O_4 Boxes for High Capacity Supercapacitor. *J. Power Sources* **2013**, *227*, 101−105.
(17) Duay, J.; Sherrill, S. A.; Gui, Z.; Gillette, E.; Lee, S. B. Self-Limiting Electrodeposition of Hierarchical MnO_2 and $M(OH)_2/MnO_2$ Nanofibril/Nanowires: Mechanism and Supercapacitor Properties. *ACS Nano* **2013**, *7*, 1200−1214.
(18) Wang, B.; Chen, J. S.; Wang, Z.; Madhavi, S.; Lou, X. W. Green Synthesis of NiO Nanobelts with Exceptional Pseudo-Capacitive Properties. *Adv. Energy Mater.* **2012**, *2*, 1188−1192.
(19) Wang, Y. Y.; Lei, Y.; Li, J.; Gu, L.; Yuan, H. Y.; Xiao, D. Synthesis of 3D-Nanonet Hollow Structured Co_3O_4 for High Capacity Supercapacitor. *ACS Appl. Mater. Interfaces* **2014**, *6*, 6739−6747.
(20) Xiao, J. W.; Wan, L.; Yang, S. H.; Xiao, F.; Wang, S. Design Hierarchical Electrodes with Highly Conductive $NiCo_2S_4$ Nanotube Arrays Grown on Carbon Fiber Paper for High-Performance Pseudocapacitors. *Nano Lett.* **2014**, *14*, 831−838.
(21) Jiang, Z.; Lu, W. J.; Li, Z. P.; Ho, K. H.; Li, X.; Jiao, X. L.; Chen, D. R. Synthesis of Amorphous Cobalt Sulfide Polyhedral Nanocages for High Performance Supercapacitors. *J. Mater. Chem. A* **2014**, *2*, 8603−8606.
(22) Yu, L.; Zhang, L.; Wu, H. B.; Lou, X. W. Formation of $Ni_xCo_{3-x}S_4$ Hollow Nanoprisms with Enhanced Pseudocapacitive Properties. *Angew. Chem., Int. Ed.* **2014**, *53*, 3711−3714.
(23) Chen, H.; Jiang, J.; Zhang, L.; Wan, H.; Qi, T.; Xia, D. Highly Conductive $NiCo_2S_4$ Urchin-like Nanostructures for High-Rate Pseudocapacitors. *Nanoscale* **2013**, *5*, 8879−8883.
(24) Yang, J. Q.; Duan, X. C.; Qin, Q.; Zheng, W. J. Solvothermal Synthesis of Hierarchical Flower-like Beta-NiS with Excellent Electrochemical Performance for Supercapacitors. *J. Mater. Chem. A* **2013**, *1*, 7880−7884.
(25) Zhang, L.; Wu, H. B.; Lou, (D.) X. W. Unusual CoS_2 Ellipsoids with Anisotropic Tube-like Cavities and Their Application in Supercapacitors. *Chem. Commun.* **2012**, *48*, 6912−6914.
(26) Chen, W.; Xia, C.; Alshareef, H. N. One-Step Electrodeposited Nickel Cobalt Sulfide Nanosheet Arrays for High-Performance Asymmetric Supercapacitors. *ACS Nano* **2014**, *8*, 9531−9541.
(27) Wu, H. B.; Pang, H.; Lou, (D.) X. W. Facile Synthesis of Mesoporous $Ni_{0.3}Co_{2.7}O_4$ Hierarchical Structures for High-Performance Supercapacitors. *Energy Environ. Sci.* **2013**, *6*, 3619−3626.
(28) Tang, S. C.; Vongehr, S.; Wang, Y. G.; Cui, J.; Wang, X. Y.; Meng, X. K. Versatile Synthesis of High Surface Area Multi-Metallic Nanosponges Allowing Control over Nanostructure and Alloying for Catalysis and SERS Detection. *J. Mater. Chem. A* **2014**, *2*, 3648−3660.
(29) Huang, Y.; Liang, J. J.; Chen, Y. S. An Overview of the Applications of Graphene-Based Materials in Supercapacitors. *Small* **2012**, *8*, 1805−1834.
(30) Worsley, M. A.; Pham, T. P.; Yan, A. M.; Shin, S. J.; Lee, J. R. I.; Bagge-Hansen, M.; Mickelson, W.; Zettl, A. Synthesis and Characterization of Highly Crystalline Graphene Aerogels. *ACS Nano* **2014**, *8*, 11013−11022.
(31) Lee, J. H.; Park, N.; Kim, B. G.; Jung, D. S.; Im, K.; Hur, J.; Choi, J. W. Restacking-Inhibited 3D Reduced Graphene Oxide for High Performance Supercapacitor Electrodes. *ACS Nano* **2013**, *7*, 9366−9374.
(32) Lu, T.; Zhang, Y. P.; Li, H. B.; Pan, L. K.; Li, Y. L.; Sun, Z. Electrochemical Behaviors of Graphene−ZnO and Graphene−SnO_2 Composite Films for Supercapacitors. *Electrochim. Acta* **2010**, *55*, 4170−4173.
(33) Beberwyck, B. J.; Alivisatos, A. P. Ion Exchange Synthesis of III−V Nanocrystals. *J. Am. Chem. Soc.* **2012**, *134*, 19977−19980.
(34) Li, J. F.; Xiong, S. L.; Liu, Y. R.; Ju, Z. C.; Qian, Y. T. High Electrochemical Performance of Monodisperse $NiCo_2O_4$ Mesoporous Microspheres as an Anode Material for Li-Ion Batteries. *ACS Appl. Mater. Interfaces* **2013**, *5*, 981−988.
(35) Zhang, B.; Ye, X. C.; Dai, W.; Hou, W. Y.; Xie, Y. Biomolecule-Assisted Synthesis and Electrochemical Hydrogen Storage of Porous Spongelike Ni_3S_2 Nanostructures Grown Directly on Nickel Foils. *Chem.—Eur. J.* **2006**, *12*, 2337−2342.
(36) Yua, D. B.; Wang, Y. l.; Zhang, L.; Low, Z. X.; Zhang, X. Y.; Chen, F. L.; Feng, Y.; Wang, H. T. Three-Dimensional Branched Single-Crystal β-$Co(OH)_2$ Nanowire Array and Its Application for Supercapacitor with Excellent Electrochemical Property. *Nano Energy* **2014**, *10*, 153−162.
(37) Li, J. K.; Xiao, J. W.; Wang, Z. L.; Wei, Z. H.; Qiua, Y. C.; Yang, S. H. Construction of Bicontinuously Porous Ni Architecture as a Deposition Scaffold for High Performance Electrochemical Supercapacitors. *Nano Energy* **2014**, *10*, 329−336.
(38) Li, M.; Xu, S. H.; Liu, T.; Wang, F.; Yang, P. X.; Wang, L. W.; Chu, P. K. Electrochemically-Deposited Nanostructured $Co(OH)_2$ Flakes on Three-Dimensional Ordered Nickel/Silicon Microchannel Plates for Miniature Supercapacitors. *J. Mater. Chem. A* **2013**, *1*, 532−540.
(39) Yan, T.; Li, Z. J.; Li, R. Y.; Ning, Q.; Kong, H.; Niu, Y. L.; Liu, J. K. Nickel−Cobalt Double Hydroxides Microspheres with Hollow Interior and Hedgehog-like Exterior Structures for Supercapacitors. *J. Mater. Chem.* **2012**, *22*, 23587−23592.

DOI: 10.1021/am508747m
ACS Appl. Mater. Interfaces 2015, 7, 4311−4319

(40) Zhou, G. M.; Wang, D. W.; Li, F.; Zhang, L. L.; Li, N.; Wu, Z. S.; Wen, L.; Lu, G. Q.; Cheng, H. M. Graphene-Wrapped Fe_3O_4 Anode Material with Improved Reversible Capacity and Cyclic Stability for Lithium Ion Batteries. *Chem. Mater.* **2010**, *22*, 5306−5313.
(41) Cheng, D. P.; Khan, M. A.; Houser, R. P. Structural Variability of Cobalt(II) Coordination Polymers: Three Polymorphs of $Co_3(TMA)_2$ [TMA = Trimesate, $C_6H_3(COO)_3^{3-}$]. *Cryst. Growth Des.* **2004**, *4*, 599−604.
(42) Du, W. M.; Wang, Z. Y.; Zhu, Z. Q.; Hu, S.; Zhu, X. Y.; Shi, Y. F.; Pang, H.; Qian, X. F. Facile Synthesis and Superior Electrochemical Performances of $CoNi_2S_4$/Graphene Nanocomposite Suitable for Supercapacitor Electrodes. *J. Mater. Chem. A* **2014**, *2*, 9613−9619.
(43) Pang, H.; Wei, C. Z.; Li, X. X.; Li, G. C.; Ma, Y. H.; Li, S. J.; Chen, J.; Zhang, J. S. Microwave-Assisted Synthesis of NiS_2 Nanostructures for Supercapacitors and Cocatalytic Enhancing Photocatalytic H_2 Production. *Sci. Rep.* **2014**, *4*, 3577.
(44) Du, W. M.; Zhu, Z. Q.; Wang, Y. B.; Liu, J. N.; Yang, W. J.; Qian, X. F.; Pang, H. One-Step Synthesis of $CoNi_2S_4$ Nanoparticles for Supercapacitor Electrodes. *RSC Adv.* **2014**, *4*, 6998−7002.
(45) Mi, L. W.; Chen, Y. F.; Wei, W. T.; Chen, W. H.; Hou, H. W.; Zheng, Z. Large-Scale Urchin-like Micro/Nano-Structured NiS: Controlled Synthesis, Cation Exchange and Lithium-Ion Battery Applications. *RSC Adv.* **2013**, *3*, 17431−17439.

DOI: 10.1021/am508747m
ACS Appl. Mater. Interfaces 2015, 7, 4311−4319